

New Cyanide-Free Ammonia Bath for Brass Alloy Coatings on Steel Substrate by Electrodeposition

Magdy A.M.Ibrahim^{1,2,*}, Rashed S. Bakdash¹

¹ Chemistry Department, Faculty of Science, Taibah University, Al Maddinah Al Mounwara, 30002 KSA

² Chemistry Department, Faculty of Science, Ain Shams University, Abbassia, Cairo, 11566 Egypt

*E-mail: imagdy1963@hotmail.com

Received: 15 April 2015 / Accepted: 18 August 2015 / Published: 30 September 2015

The electrodeposition of highly adherent brass alloy coating onto steel substrate was successfully achieved using a cyanide-free ammonia solution. Ammonia solution forms soluble complexes with both Zn^{2+} and Cu^{2+} ions with high stability constants. The bath composition necessary to obtain smooth and highly adherent red brass alloy contains: $CuSO_4 \cdot 5H_2O$ 30 g/L, $ZnSO_4 \cdot 7H_2O$ 30 g/L, NH_3 88ml /L, $(NH_4)_2SO_4$ 50 g/L, KOH 20 g/L, pH 9.65, $t = 15$ min., $i = 0.12$ Adm^{-2} and at $20^\circ C$. The investigations were carried out using voltammetric techniques such as; potentiodynamic cathodic polarization curves, anodic linear stripping voltammetry and cyclic voltammetry. The zinc content in the brass alloy deposits was ranged from 5-18.5 wt%. The cyclic voltammetric data indicating that the rate of growth is controlled by mass transfer of copper and zinc ions to the growing center. The first stage of nucleation and growth of brass alloy fit the model of three dimensional instantaneous nucleation. The brass deposit was characterized by XRD and SEM measurements.

Keywords: Brass alloy, Cyclic voltammetry, XRD analysis, Chronoamperometry, Ammonia

1. INTRODUCTION

Brass is an alloy made of copper and zinc; the ratios of zinc and copper can be changed to produce a range of brasses with different properties. For example, α - brass contains less than 35% zinc, can be use in pressing. β - brass, contains 45–50% zinc, can be suitable for casting. While α - β brass, or duplex brass contains 35–45% zinc and is suited for hot working. However, there are other brass alloys which did not take enough attention. One of them is the rich low brass which contains 5-20% zinc, often used for jewelry. Therefore, brass alloys have many applications in industry, due to their valuable attractive properties such as their mechanical and corrosion resistance, household appliances,

adhesion of rubber to steel, in addition to their decorative value [1-4]. Brass plating of aircraft engine parts was used to reduce friction [5]. It is recommended that, using complexing agents produce high quality metallic alloy coatings [6]. The complexing agent decreases the concentration of the more noble ion in solution. Unfortunately, brass alloy has been deposited commercially only from cyanide complex baths in spite of their toxicity and their difficulty in maintenance. Eco-friendly electroplating processes gain permanently enhanced attention and several non-cyanide baths have been developed such as: pyrophosphate [6,7], glucoheptonate [8], EDTA [4], gluconate [9], sorbitol [10], citrate [11,12], tartrate [13,14], glycine [14] and D-mannitol [3] baths. Moreover, Cu-Zn alloy has been deposited from ionic liquid at room temperature [1,2]. However, such alloys have not been applied commercially, since the coatings do not adhere well and show bad coloration. Resistivity values for Cu-Zn alloy prepared by electrodeposition are as a rule approximately 25 to 45 percent higher than the resistivities of the corresponding metallurgical alloys [15]. The alkaline ammonical baths have been used in our Lab for metal deposition because they have good throwing power, high bath stability for a long time and the deposit exhibits a well adherence to the metal substrate [16,17]. Therefore, the present work aims to develop new bath based on ammonia solution, for producing good quality brass alloy deposits.

2. EXPERIMENTAL

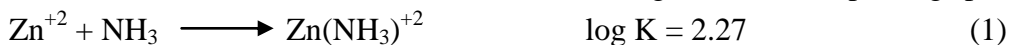
The composition of the tested bath of the alloy deposition contains: $\text{CuSO}_4 \cdot 5\text{H}_2\text{O}$ 30 g/L, $\text{ZnSO}_4 \cdot 7\text{H}_2\text{O}$ 30 g/L, NH_3 88 ml /L, $(\text{NH}_4)_2\text{SO}_4$ 50 g/L, KOH 20 g/L, pH 9.65 and at 20°C. The conductivity of this solution was 72.5 mS cm^{-1} . A steel and platinum sheets each of dimensions 2.5 cm x 3.0 cm were used as cathode and anode for brass electroplating, respectively. The electroplating cell used was a trough made of Perspex. The steel substrate was cleaned mechanically by polishing it using different grade emery papers 600, 800, 1000 and 1500 and then washed with distilled water, rinsed with ethanol and weighed. The plating time was 15 min at a temperature of $20^\circ\text{C} \pm 2$. The composition of the alloy was determined by Energy dispersive X-ray (Philips Model: XL-40FEG field emission). The surface morphology of brass alloy was studied using a scanning electron microscopy (JOEL- JCM 6000). The phase and the crystal structure of brass alloys was analyzed by x-ray diffraction (shimadzu Model: 6000 LabX) using a diffractometer (40 kV 20 mA) with a Ni filter and Cu $K\alpha$ radiation. The polarization curves were recorded using steel cathode by scanning the potential to the more negative potential values with scan rate of 10 mVs^{-1} . All of the electrochemical experiments were carried out using a computer assisted potentiostat/galvanostat (SI 1287 Solartron). The potentials were measured relative to a saturated calomel electrode (SCE). In the in situ-anodic linear stripping voltammetry (ALS) measurements, the deposition of brass alloy from the plating bath was carried out at a certain deposition potential for a certain plating time. After the deposition process on the GCE, anodic stripping analysis was performed quickly in the same plating bath (i.e. in situ) by sweeping the potential to the more anodic potentials at a constant sweep rate of 10 mV s^{-1} . The chronoamperometry (current–time transients) measurement was carried out at different applied potentials. The brass was

deposited at a certain constant potential and the relationship between the current and time was recorded for 30 seconds.

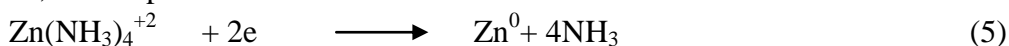
3. RESULTS AND DISCUSSION

3.1. Chemistry of ammonia with Cu^{2+} and Zn^{2+} ions

Ammonia reacts with Zn^{2+} ions in solution forming different complexing species[18]:



According to the equilibrium constants of the NH_3 complexes of zinc, only $\text{Zn}(\text{NH}_3)_3^{+2}$ and $\text{Zn}(\text{NH}_3)_4^{+2}$ could be considered because of their high stability constants. Moreover, for the considered concentration of $\text{NH}_3/\text{NH}_4^+$ species, the complexes were stable over a broad pH range. In acidic media ($\text{pH} < 6.4$) free zinc ions were shown to predominate. However, $\text{Zn}(\text{NH}_3)_3^{+2}$ existed in the narrow pH range of 6.3 to 6.6 and $\text{Zn}(\text{NH}_3)_4^{+2}$ was the major form for pH values ranging from 6.6 to 13.1. Therefore, zinc deposition from the ammonia bath can be considered as:



On the other hand, ammonium ions form soluble complexes with copper ions. The complex formed depends on the pH values. In the pH range $7.7 < \text{pH} < 1.9$, Cu^{2+} ions predominate as $\text{Cu}(\text{NH}_3)_4^{+2}$. Copper complexation in the ammonia bath [17], therefore, is



Therefore, it is clear that the stability constant of the copper ammine complex is higher than that of zinc ammine complex. Copper deposition from the ammonia bath can therefore be considered as:



Reduction of the copper amine complex or zinc amine complex is not as easy as the reduction of the free Cu^{2+} or Zn^{2+} ions.

Moreover, the zinc and copper solutions contains ammonium sulphate in addition to ammonia solution, and therefore, H^+ can be produced according to the following equilibrium [19]:



The formation of such complexes species decreases the concentration of the electroactive free copper and zinc species. As ammine complexes of copper and zinc are formed, it would be expected that the complex formation might affect the electrochemical reduction behavior of Cu^{2+} and Zn^{2+} in the bath, therefore, codeposition of copper and zinc can be realized by complex formation. In the present study, the ammonium ions is useful for controlling the color of the brass deposit, acts as a complexing agent, assists in good anode dissolution (in case of soluble anode) and acts as a means of pH control [5].

3.2. Surface morphology and microstructure of brass alloy

The electrodeposition of brass alloy has been carried out successfully onto steel substrate using the following bath composition: $\text{CuSO}_4 \cdot 5\text{H}_2\text{O}$ 30 g/L, $\text{ZnSO}_4 \cdot 7\text{H}_2\text{O}$ 30 g/L, NH_3 88 ml /L, $(\text{NH}_4)_2\text{SO}_4$ 50 g/L, KOH 20 g/L, pH 9.65, Temp. =20°C, t = 15 min, and $i = 0.12 \text{ Adm}^{-2}$. KOH is normally added to increase the electrical conductivity of the bath. The brass alloy produced from this bath has a red colour and is characterized by a good adherence to the steel substrate. The adhesion tests were carried out by the bent as well as by the heat-quench methods. The zinc content in the brass alloy was in the range of 5-18.5 wt% depending on the operating conditions. This means that the brass alloy produced could be classified as high low rich brass alloy. The surface morphology of the brass electrodeposited from the above mentioned bath is shown in Fig. 1.

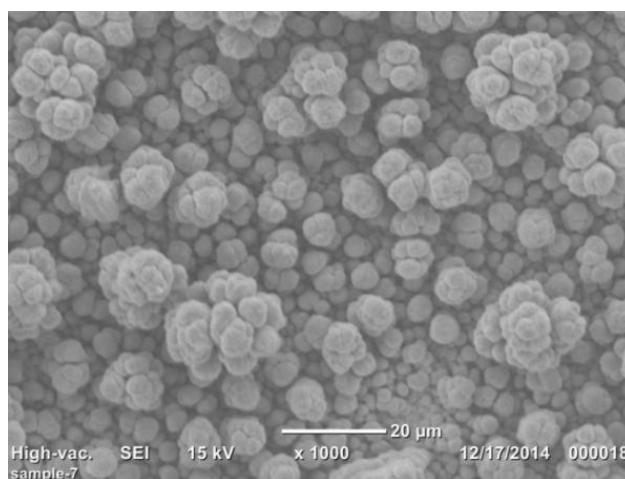


Figure 1. The surface morphology of brass alloy (12.5% Zn)

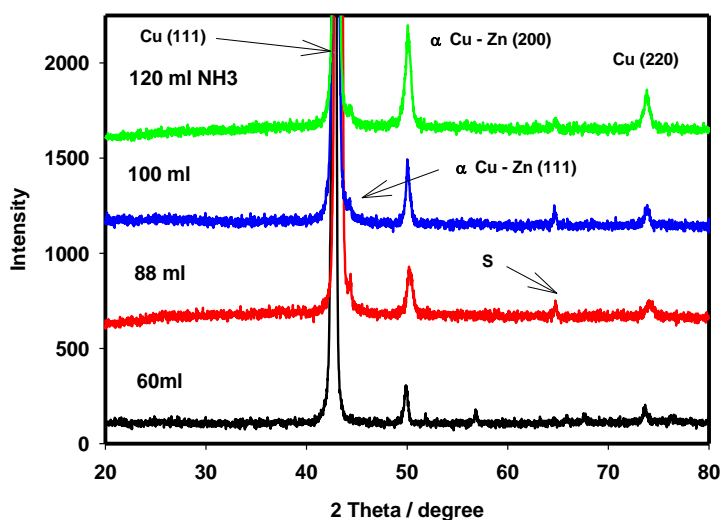


Figure 2. X-ray diffraction analysis of brass deposits in the presence of different concentrations of ammonia solution

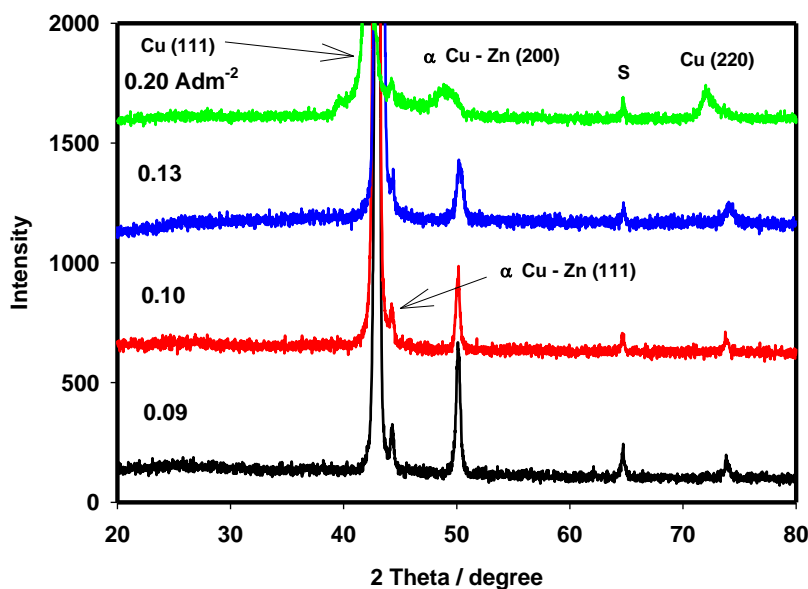


Figure 3. X-ray diffraction analysis of brass deposits at different current density

The SEM photomicrograph exhibits a flower-like structure of different sizes, completely covered the entire cathode surface and are free from cracking. Similar morphology of brass deposits was recorded during the electrodeposition of Cu–Zn alloy from room temperature ionic liquid [1]. It is worthwhile to mention that this cyanide-free ammonia bath is working well at room temperature. However, raising the bath temperature $> 30^{\circ}\text{C}$ led to the formation of very poor deposits on the steel substrate. It was found that at temperature $\geq 50^{\circ}\text{C}$, no deposition of copper takes place from ammonia bath [17]. Similarly, the efficiency of zinc deposition from ammonia bath was decreased gradually with raising the bath temperature [16].

Figs. 2 and 3 show typical X-ray diffraction pattern of brass deposits obtained at the steel substrate at various ammonia concentrations and at various current densities respectively. The XRD patterns shows a strong reflection peak at $2\theta = 41.8^{\circ}$ corresponding to the Cu(111) and another peak at $2\theta = 50^{\circ}$ corresponding to α -CuZn (200) in addition to a weak shoulder at $2\theta = 45^{\circ}$ corresponding to α -CuZn (111) [3]. This means that the alloy phase composition and structure of the Cu-Zn alloy deposited from the present alkaline ammonical solution presents α - phase with a fcc lattice. It is reported in the literature [20] that cyanide-free electrolytes mainly produce deposits of metallic copper and zinc oxide or hydroxide. However, the XRD results for the brass deposits obtained from alkaline ammonical bath did not indicate elemental zinc or zinc oxide or hydroxide. The diffractograms of the brass deposits using different concentrations of ammonia as a complexing agents indicated an increase in the peak intensity at $2\theta = 50^{\circ}$ for the Cu-Zn phase alloy. On the other hand, Fig. 3 shows a decrease in this peak intensity with increasing the current density indicating that it becomes less crystalline or in other word more amorphous. This result is in good agreement with the reported conclusion that in the copper-rich Cu-Zn, alloy presents α - phase with a fcc lattice or zinc solid solution in copper [3].

3.3. Voltammetric behavior

3.3.1. Potentiodynamic cathodic polarization curves

The criteria for simultaneous deposition of two metals as an alloy are that their potentials be close and that their cathodic polarizations be such that deposition occurs at the desired ratio. Therefore, the potentiodynamic cathodic polarization (i - E) curves for the individual depositions of copper, zinc and brass alloy from the ammonia baths recorded under similar conditions were measured and the results are shown in Fig. 4.

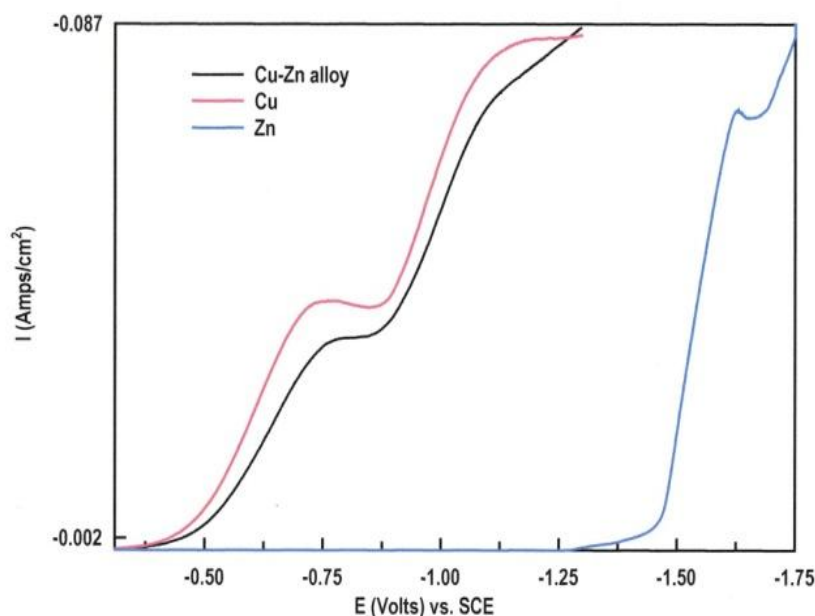


Figure 4. Polarization curves onto steel for pure Cu, Zn and brass alloy under similar conditions

The curves were swept linearly from the rest potentials to the more negative direction with a scan rate of 10 mVs^{-1} . The alloy polarization curve lies between the Cu and Zn polarization curves. Several alloys show similar relationship of their polarization curves during electrodeposition [21-23]. Inspection of the data reveals that the polarization curves for Cu and Cu-Zn alloy are similar to each other. Each curve exhibits two limiting current plateaus. In brass alloy the limiting current density was lower than that of pure copper. Under limiting conditions, alloy codeposition proceeds via mass transport control and the deposition of rich –copper alloys would be expected. The second limiting current at high current and high potentials could be attributed to the H_2 evolution. On the other hand, the copper polarization curve was at less negative potentials than the zinc curve, indicating that copper is the nobler metal in the system. Therefore one can expect preferential deposition of copper (normal deposition) and consequently producing copper-rich alloys.

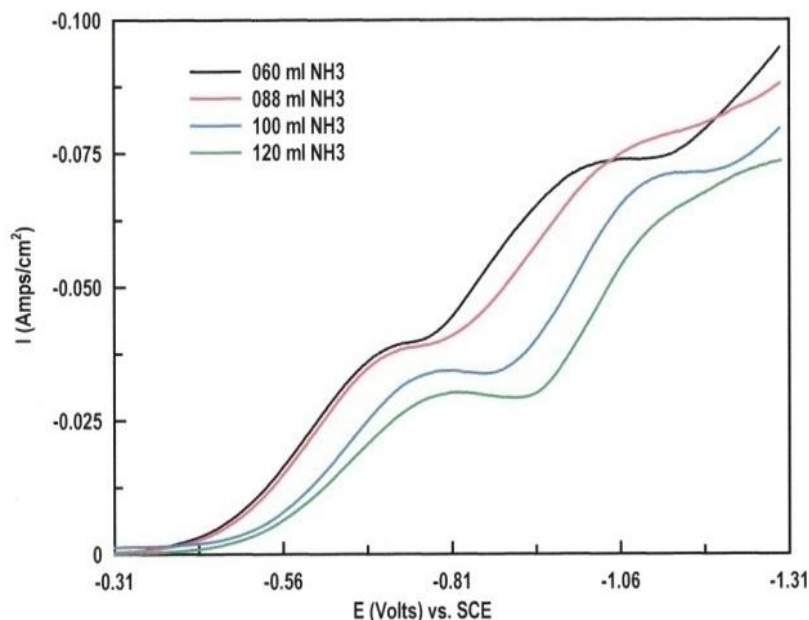


Figure 5. Polarization curves of brass alloy deposition at different concentrations of ammonia solution

The effect of ammonia concentration on the polarization curves was studied and the results are shown in Fig. 5. The data show that the cathodic polarization curves of brass alloy deposition increases with increasing ammonia concentration. On other words, the overpotential increases due to a decrease in the concentration of free Cu^{2+} and Zn^{2+} ions when the complexing agent content is increased. This is mainly attributable to the increased stability of Cu and Zn amine complexes. Since, the reduction from the complexed species is not so easy as the reduction from the free Cu^{2+} and Zn^{2+} ions. Moreover, the two limiting current densities were decreased significantly with increasing the ammonia concentration.

3.3.2. Cyclic voltammetry

A typical cyclic voltammograms of brass alloy recorded at a glassy carbon electrode using the ammonia bath under the influence of increasing the scan rate ($25\text{-}100\text{ mVs}^{-1}$), is shown in Fig. 6. The cyclic voltammogram exhibits two distinct voltammetric peaks corresponding to the simultaneous reduction of Cu^{2+} and Zn^{2+} ions to the brass alloy (peak I) and the oxidation of the alloy formed (peak II) respectively. The relationship between the cathodic current peak (i_{cp}) and the square root of the scan rate ($v^{1/2}$) (Fig. 7) was found to be linear, indicating that the rate of growth is controlled by mass transfer of copper and zinc to the growing center [24]. On the other hand, the negative value of the cathodic current peak density i_{cp} at $v^{1/2} = 0$, is consistent with a deposition process involving a nucleation mechanism controlled by mass transfer [25].

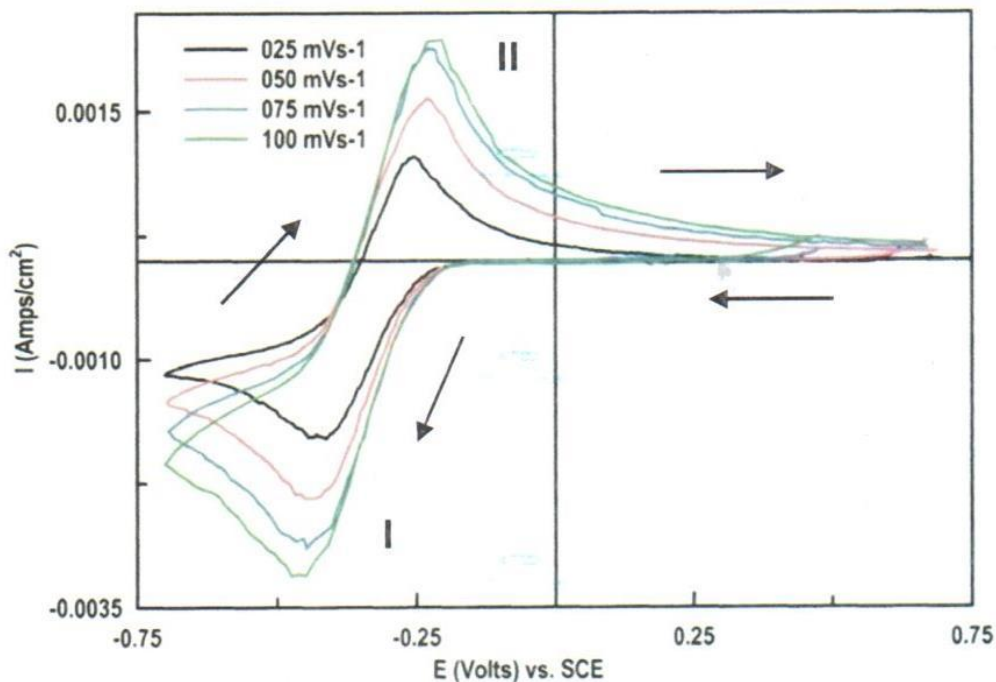


Figure 6. Cyclic voltammtric curves recorded at GCE at different scan rates

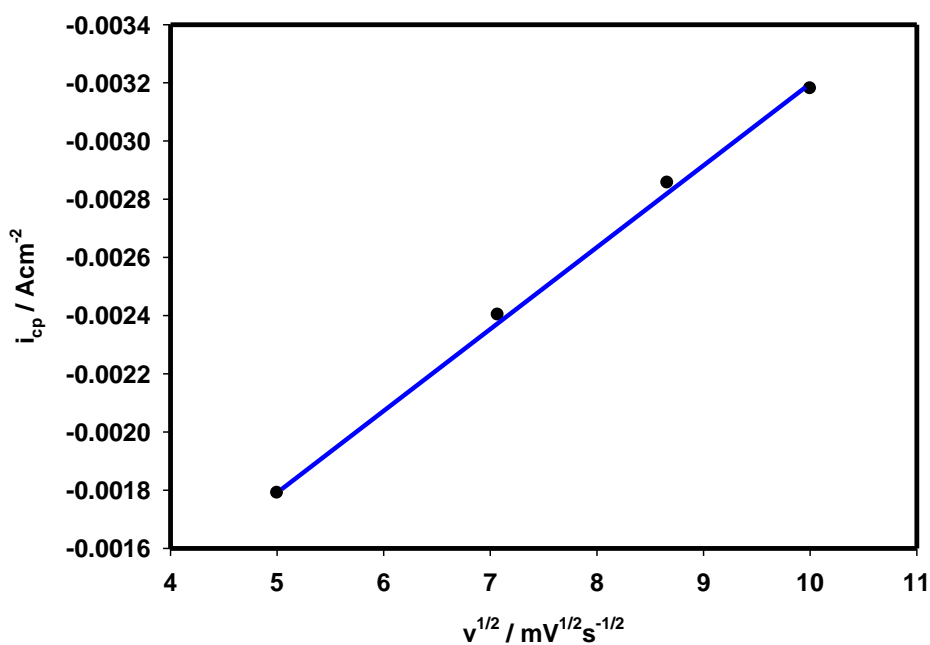


Figure 7. Plot of i_{cp} vs. $v^{1/2}$

3.3.3. Anodic linear stripping voltammetry

A typical in-situ anodic linear stripping voltammograms for brass alloy codeposited on GCE at different plating conditions are shown in Figs. 8 and 9.

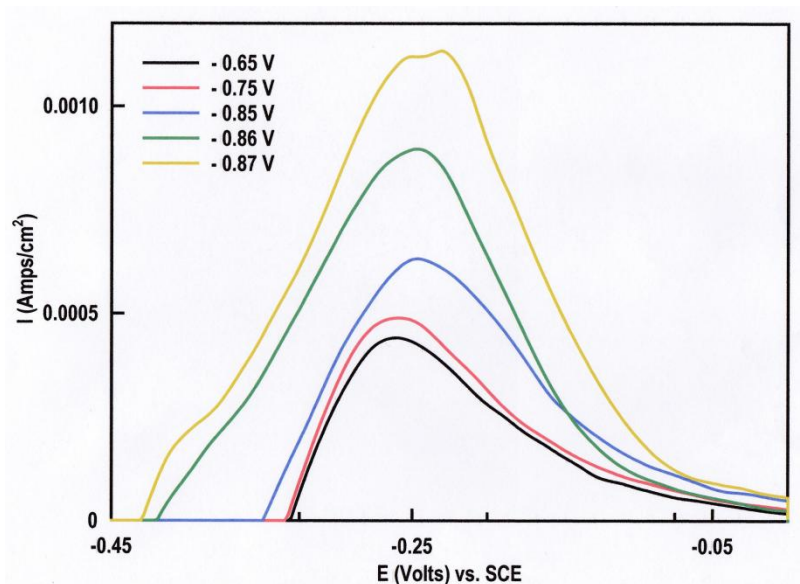


Figure 8. ALSV curves recorded at GC electrode at different applied potentials

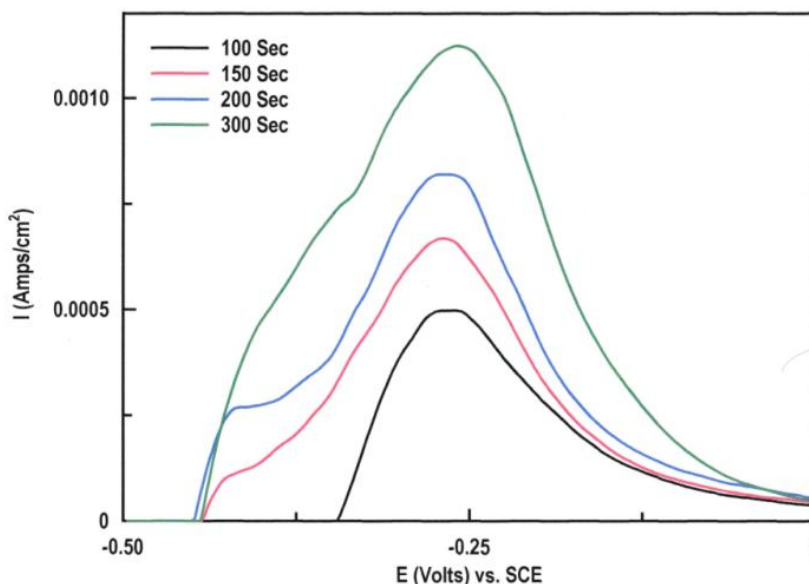


Figure 9. ALSV curves recorded at GC electrode at different plating time

The alloy was deposited at a certain deposition potential for a certain time. Immediately, after deposition, the potential was moved in the noble direction at a scan rate of 10 mVs^{-1} and an anodic stripping voltammogram was recorded without moving the electrode from the solution i.e. in situ measurements. Each voltammogram contains a single dissolution peak. The appearance of only one dissolution peak for brass alloy indicates that the Cu and Zn components of the alloy dissolved simultaneously. Moreover, the presence of a single anodic peak of brass alloy denotes that the alloy consists of one phase (solid solution) [25]. However, the anodic stripping charge (the area under the peak) can estimate the cathodic current efficiency of the deposition process. Fig. 8 depicts the effect of

alloy deposition potential on the anodic stripping response of alloy plating solution. As the deposition potential was made more negative, the height and the area under the stripping peak increased and the efficiency of the alloy deposition increased. On the other hand, Fig.9 reveals that the stripping charge was enhanced with increasing the deposition time, indicating that the current efficiency of the alloy deposition increased with increasing the plating time.

3.4. Chronoamperometric analysis

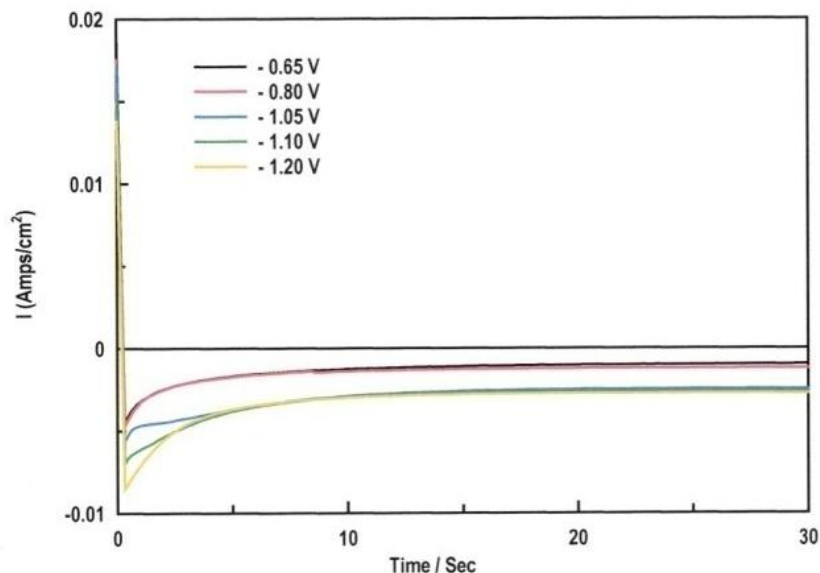


Figure 10. Current-time transients curves recorded at GC electrode at different deposition potentials

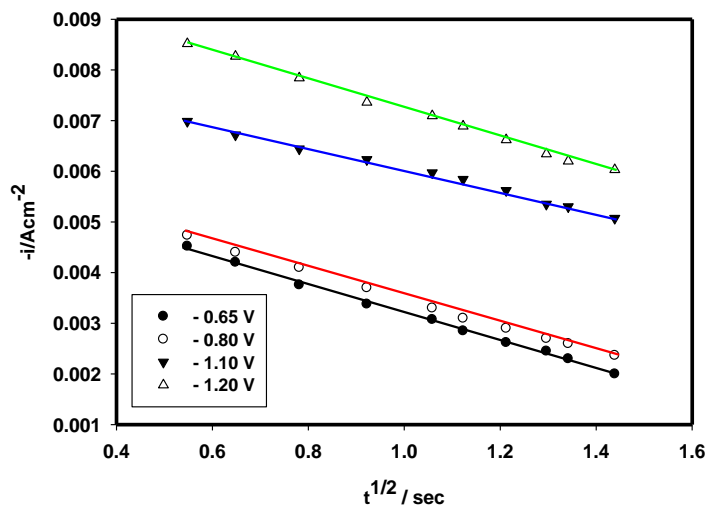


Figure 11. Plotting i versus $t^{1/2}$ at different potentials

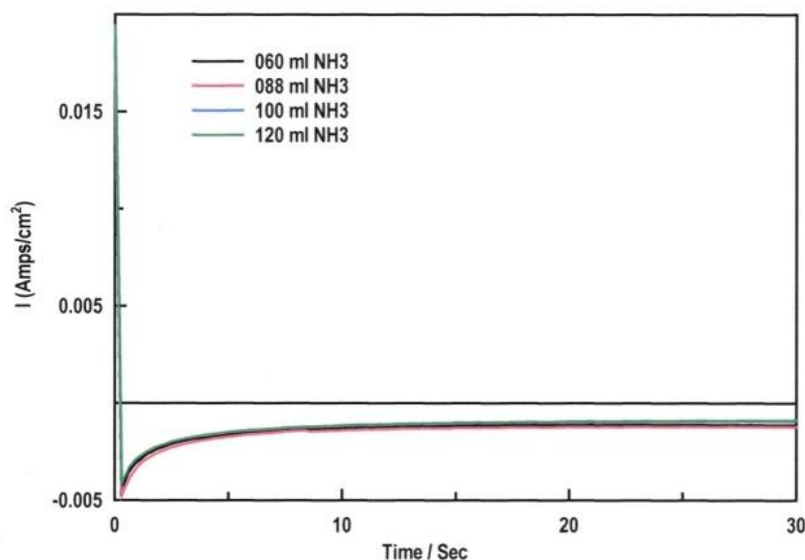


Figure 12. Current-time transients curves recorded at GC electrode at different ammonia concentrations

To get more information about the first stage of nucleation and growth mechanism of brass alloy deposition, chronoamperometric analysis (current-time transient) were recorded. Fig. 10 shows the current-time transients recorded during the electrodeposition of brass alloy at different deposition potentials. The current-time curves can be divided into three regions. In the first region, which corresponds to short times, the decrease in the cathodic current density is related to the charging of the electric double layer [26]. In the second region the current increased slightly as a result of alloy nucleation and growth on the steel substrate. Finally, the current density is reached to a steady state. As the deposition potential is made more negative, the values of the instantaneous and steady-state current increase. For the ascending parts of the current transients, if the current density i is plotted versus $t^{1/2}$ a straight lines was obtained (Fig. 11).

The slopes of the lines depend on the value of the deposition potential. This indicates that under such conditions, instantaneous 3D growth of brass alloy nucleation occurs. If the mechanism follows instantaneous growth the number of nuclei on the surface instantaneously reaches the saturation. Fig. 12 show that changing the NH_3 concentration has no significant effect on the i - t transient i.e., has no significant effect on the initial nucleation of the alloy deposition process.

4. CONCLUSIONS

Highly adherent brass coatings on copper substrates from an alkaline ammonical complexing bath were successfully produced by electrodeposition. The bath composition necessary to obtain smooth and highly adherent red brass alloy contains: $\text{CuSO}_4 \cdot 5\text{H}_2\text{O}$ 30 g/L, $\text{ZnSO}_4 \cdot 7\text{H}_2\text{O}$ 30 g/L, NH_3 88 ml /L, $(\text{NH}_4)_2\text{SO}_4$ 50 g/L, KOH 20 g/L, pH 9.65, $t = 15$ min., $i = 0.12 \text{ Adm}^{-2}$ and at 20°C . The Zn% in the brass alloy deposits was ranged from 5-18.5 wt%. XRD-analysis showed that the brass alloy

presents α - phase with fcc lattice. Cyclic voltammetry proved that the deposition process involved a nucleation mechanism controlled by mass transfer. The first stage of nucleation and growth of brass alloy fit the model of 3-D nucleation.

References

1. C. Rouse, S. Beaufile, and P. Fricoteaux, *Electrochim. Acta*, 107 (2013) 624.
2. P.D. Vreese, A. Skoczylas, E. Matthijs, J. Fransaer, and K. Binnemans, *Electrochim. Acta*, 108 (2013) 780.
3. R. Juskenas, V. Karpaviciene, V. Pakstas, A. Selskis, and V. Kapocius, *J. Electroanal. Chem.*, 602 (2007) 237.
4. M.R.H. De Almeida, E.B. Barbano, M.F. De Carvalho, I.A. Carlos, J.L.P. Siqueira, and L.L. Barbosa, *Surf. Coat. Technol.*, 206 (2011) 95.
5. F.A. Lowenheim, "Modern Electroplating" Wiley, New York (1963)
6. L.F. Senna, S.L. Diaz, and L. Sathler, *J. Appl. Electrochem.*, 33 (2003) 1155.
7. K. Johannsen, D. Page, and S. Roy, *Electrochim. Acta.*, 45 (2000) 3691.
8. Y. Fujiwara, H. Enomoto, *Surf. Coat. Technol.*, 35 (1988) 101.
9. E.G. Vinokurov, K.L. Kandyrin, and V.V. Bondar, *J. Appl. Electrochem.*, 83 (2010) 659.
10. I.A. Carlos, and M.R.H. De Almeida, *J. Electroanal. Chem.*, 562 (2004) 153.
11. F.L.G. Silva, D.C.B. Do Lago, E. Delia, L.F. Senna, *J. Appl. Electrochem.*, 40 (2010) 2013.
12. F.B.A. Ferreira, F.L.G. Silva, A.S. Luna, D.C.B. Lago, and L.F. Senna, *J. Appl. Electrochem.*, 37 (2007) 473.
13. S.S. Abd El Rehim, and M.E. El Ayashy, *J. Appl. Electrochem.*, 8 (1978) 33.
14. S.M. Rashwan, *Trans. Inst. Met. Finish.*, 85 (2007) 217.
15. W.H. Safranek, "The Properties of Electrodeposited Metals and Alloys.", American Elsevier Publishing Co., INC (1974)
16. M. A. M. Ibrahim, *J. Appl. Surf. Finish.*, 3 (2) (2008) 89.
17. M. A. M. Ibrahim, MAM, *Plat. Surf. Finish.*, 87 (2000) 67.
18. J. Bjerrum, ph.D. Dissertation, Copenhagen (1941); reprinted by P. Haase & Son, Copenhagen, 1957.
19. S. Kotrly, and L. Suche, Handbook of Chemical Equilibria in Analytical Chemistry, Ellis Horwood, Chichester, UK (1985).
20. T. Vagramyan, J.S.L. Leach, J.R. Moon, *Electrochim. Acta*, 24 (1979) 231.
21. S.S. Abd El Rehim, M.A.M. Ibrahim, S.M. Abd El Wahaab, M.M. Dankeria, *Trans. Inst. Met. Finish.*, 77 (1999) 31.
22. S.S. Abd El Rehim, M.A.A. Ibrahim, *Met. Finish.*, 96 (1998) 65.
23. M.A.M. Ibrahim, S.S. Abd El Rehim, M.M. El Naggar, M.A. Abbass, *J. Appl. Surf. Finish.*, 1 (2006) 293.
24. T. Otero, and J. Rodriguez-Jimenez, *J. Appl. Electrochem.*, 29(2) (1999) 239.
25. G.J. Hills, D.J. Schiffrin, J. Thompson, *Electrochim. Acta*, 19(11) (1974) 657.
26. M.A.M. Ibrahim, S.S. Abd El Rehim, and S.O. Moussa, *J. Appl. Electrochem.*, 33 (2003) 627.